Asian Journal of Chemistry; Vol. 30, No. 11 (2018), 2502-2508

ASIAN JOURNAL OF CHEMISTRY

https://doi.org/10.14233/ajchem.2018.21507

# Synthesis and Identification of $Co_3O_4$·$Fe_3O_4$/CaO Spinel Supported Catalyst

RAFID RYYIS ARRAQ and SALIH HADI KADHIM*

Department of Chemistry, College of Science, University of Babylon, Hilla, Iraq

*Corresponding author: E-mail: hadi197019@yahoo.com

*Received*: 9 June 2018; *Accepted*: 30 July 2018; *Published online*: 27 September 2018; AJC-19102

Spinel supported catalyst, $Co_3O_4$·$Fe_3O_4$/CaO was synthesized by co-precipitation method *via* calcination at different temperatures (450, 650 and 800 ºC). The resulting powder of prepared precursors was characterizes by X-ray diffraction, atomic force microscopy, Fourier transform infrared spectroscopy, energy dispersive X-ray spectroscopy, atomic absorption spectrophotometer and magnetic susceptibility measurements. The catalytic activity of the prepared catalyst was investigated by removal of Celestine blue B dye from the effluents of textile wastewater by adsorption and by photocatalytic degradation. The reaction was followed spectrophotometrically at $\lambda_{max}$ 644 nm.

**Keywords: Spinel $Co_3O_4$·$Fe_3O_4$/CaO, Co-precipitation method, Celestine blue.**

## INTRODUCTION

The spinel semiconductor oxide found in the formula $AB_2O_4$ for normal spinel structure, where A is a divalent cation that usually occupy the tetrahedral sites and B is a trivalent cations that normally occupy the octahedral sites in the spinel cubic structure. Another type of spinel structure is an inverse has the form $B(AB)O_4$, where B is a trivalent metal cation, half of this cation occupy the tetrahedral sites and another occupy the octahedral sites, A is divalent metal cation occupy an octahedral site in spinel [1,2]. The most interesting spinel structure materials in the magnetic and electrical field usually include iron and cobalt at various oxidation states [3-5].

The transition metal oxides which defined are compounds consist of oxygen atoms coalescence to transition metals [6,7] and used as a photocatalysis in wastewater treatment [8], these catalyst were capable of absorbing light and creating electron-hole pairs that allow electronic transition in the reaction because of the formation of positive holes, which resulted from the transfer electron from the valence band to the conduction band of semiconductor by absorbing energy from UV light, visible light or both producing an electron/hole pair ($e^-_{CB}/h^+_{VB}$) which is able to reduce and/or oxidize compound and degrade of pollutants in aqueous solution by using solid heterogeneous catalyst such as mixed metal oxides, which have wide applications as catalyst become of their high surface area, reactive sites, non-toxic and easily separated for reprocessing [9-12].

Most of the common industries process used dyes *via* textile industry to colour clothing, paper printing, pharmaceuticals, leather industries and other industry [13,14]. The different kinds of dyes and pigments cause large environmental pollution [15]. The wastes from these textiles industries lead to the water bodies coloured and chargining the natural growth activity of aqueous life-cycle by prevent sunlight and re-oxygenation ability of water [16]. Moreover, many of micro-organisms aqueous and humans organisms plague by carcinogenic and toxin if presences with these industrial dyes according to many reports [17,18]. Mostly, the dyes display a wide variety of different chemical structures based on substitute aromatic and heterocyclic compounds [19] flanked by chromophoric groups [20,21]. Numerous methods are used to removed coloured effluents to performed decolourization these involved physico-chemical and biological procedures for examples air stripping, precipitation, microfiltration, flocculation, coagulation or diverse sorption techniques usually with activated carbon despite the separation in these processes easy and can be transfer the pollutants from one to another medium but producing secondary waste products [22-24]. This normally requires other treatment of wastes and regeneration used the adsorbent, which causes more cost to the process [25] and acted as semiconductors in

the advanced oxidation process as photocatalysts which has added extensive attention for treatment of dye wastewaters due to its better degradation efficiency [26,27].

The aim of this work is to synthesize spinel supported catalyst $Co_3O_4$·$Fe_3O_4$/CaO by co-precipitation method and study of this catalyst by different spectroscopic techniques and investigated of their catalytic activity in the removal of celestine blue dye by adsorption and/or by photodegradation process.

## EXPERIMENTAL

The chemicals materials used in the synthesized supported catalysts *viz*., calcium nitrate (HIMEDIA company), cobalt nitrate (BDH) and ferric nitrate nonahydrate (HIMEDIA) with purity 99, 97, 98 % respectively were procured and used as such. Sodium hydroxide (BDH, 99 % pure), celestine blue and bismarck brown G dyes were obtained from Hilla textile factory.

**Synthesis of catalyst:** The supported spinel catalyst, $Co_3O_4$-$Fe_3O_4$/CaO was synthesized *via* co-precipitation method by mixing the equivalent weights of metal nitrates salts in the ratio (25:25:50) for cobalt, iron and calcium, respectively. These salts dissolved in 300 mL of deionized water and heated to 60-70 ºC with vigorously stirring and then added 1 M NaOH as a precipitation agent until pH of the solution reached to 10 and again heated mixture with constant stirring for 2 h. The resulting hydroxides were filtered and washed with deionized water until the pH of precipitate become natural and then dried at about 120 ºC for 24 h. The resulting solid precipitate then was crunched and transferred to furnace for calcination at different temperatures (450, 650 and 800 ºC) for 4 h at the heating rate of 10 ºC/min with passing of air atmosphere [28,29].

**Powder X-ray diffraction (PXRD):** The samples of synthesized spinel supported catalyst $Co_3O_4$·$Fe_3O_4$/CaO at different temperatures were studied by X-ray diffractometer (Shimadzu XRD-6000, Japan) with CuKα radiation at λ = 1.5406 Å for 2θ values ranging from 10-80º at voltage 40 kV and current 30 mA. The phase identification was achieved by comparing the X-ray pattern of the sample with standards in the JCPD cards. The crystalize size of the samples were calculated by using Debye Scherer equation $D = K\lambda/\cos\theta$, where D is the crystallite size (nm), K is a constant with range of 0.89-1.0 (in this measurement, k = 0.89) the broadening of diffraction line measured at half maximum intensity (in radian) [30].

**FT-IR:** The samples of supported catalyst $Co_3O_4$.$Fe_3O_4$/CaO were studied by infrared spectroscopy (IRAFFINTY-1, Germany) in the region (400-4000) $cm^{-1}$, using KBr powder [31].

**Atomic force microscopy (AFM):** The topography of supported catalysts surface were studied *via* used atomic force microscopy (AFM) (SPM-AA3000 Atomic Force Microscopy/ contact mode Angstrom Advanced INC.2005, USA) .

**Energy dispersive X-ray (EDX):** The spinel supported catalyst was subjected to energy-dispersive X-ray (EDX) from type (INCAX-act) model:51-ADD0104, resolution at 5.9 kV. This technique is a kind of X-ray spectroscopy used for the elemental analysis or chemical describable of sample depended on projection of a focused beam from electrons to obtain localized chemical analysis for the elements of the supported catalysts [32,33].

**Atomic absorption spectrophotometry (AAS):** The percentage of cobalt, iron and calcium elements in the prepared catalyst at three different temperatures (450, 650 and 800 ºC) were determined by using flame atomic absorption spectrophotometer (Atomic Absorption A-A-6300 Shimadzu, Japan).

**Magnetic properties of spinel supported catalyst:** The magnetic properties of spinel synthesized catalyst were determined by using balance susceptibility Model M-S-Auto.

**Photocatalytic and adsorption ability of prepared supported catalyst:** The activity of supported catalyst ($Co_3O_4$·$Fe_3O_4$/CaO) studied *via* adsorption ability and photocatalytic degradation of celestine blue dye, 50 ppm at maximum absorption wave length 644 nm.

**Homemade photoreaction cell components:** The photoreaction cell consists from pyrex glass with a window quarts and have radiation source lamp-Philips Holland (250 W) and has a total volume 30 mL. Prepared supported catalyst (0.05 g) and added to 30 mL of Celestine blue B dye (50 ppm) in the reaction cell, the reaction mixture was controlled at 25 ºC and initiated the reaction through adsorption only for a period of 10 min and withdrawn 2mL from the mixture. Then supply a ultraviolet radiation on the reaction mixture for 60 min and withdrawn 2 mL periodically from the reaction mixture after each 10 min until the reaction time finished. The samples was then compiled and centrifuged carefully to prevent any large particles formation with the supernatant liquid. The absorbance was then recorded at 644 nm for celestine blue B dye by using UV-visible double beam spectrophotometer (Shimadzu 6100 PC, Germany).

## RESULTS AND DISCUSSION

**X-ray diffraction:** The XRD patterns of prepared spinel supported catalysts ($Co_3O_4$·$Fe_3O_4$/CaO) indicated beginning the formation of desired phase at low temperature 450 ºC and completed at 650 ºC ,while at high temperature 800 ºC begin the dispersion of oxides and can be noted this by presence of different peaks due to the crystallite structure for supported catalyst was increased with increased of calcination temperature and formation the spinel type $CoFe_2O_3$/CaO (Fig. 1), in addition to that the particle size that which was measured by Debye- Scherer equation for these supported catalysts were increased with elevation temperatures (Table-1). Moreover, some deviations were noted in positions of the peaks and *d*-spacing *via* comparison with standard values from Joint Committee on

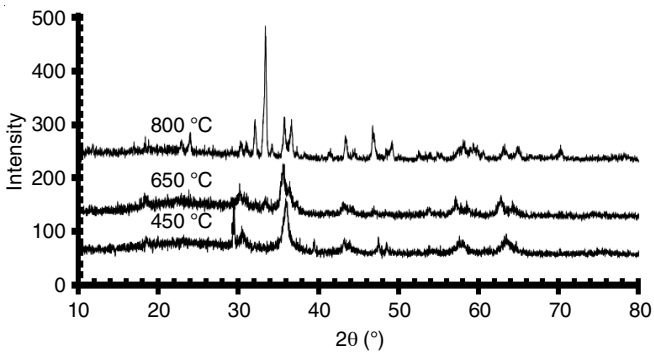


Fig. 1. XRD patterns for the prepared supported catalyst after calcination at different temperatures 450, 650 and 800 °C

TABLE-1
XRD VALUES AND CRYSTALLINE SIZE OF SUPPORTED CATALYSTS $Co_3O_4$·$Fe_3O_4$/CaO

| Sample | Temp. (°C) | 2θ (°) | d (Å) | $I/I_0$ | Full width Half maximum (β) | Average crystalline size (nm) |
|---|---|---|---|---|---|---|
| 1 | 450 | 30.2230 | 2.95476 | 28 | 0.56000 | 12.17 |
| | | 35.6173 | 2.51865 | 100 | 0.70000 | |
| | | 36.3167 | 2.47173 | 52 | 0.80000 | |
| | | 62.7634 | 1.47925 | 41 | 0.60000 | |
| | | 57.1653 | 1.61007 | 35 | 0.60000 | |
| 2 | 650 | 29.4473 | 3.03080 | 60 | 0.39330 | 15.18 |
| | | 30.5426 | 2.92456 | 28 | 0.66000 | |
| | | 35.9470 | 2.49630 | 100 | 0.64000 | |
| | | 63.3932 | 1.46606 | 25 | 0.94000 | |
| | | 43.2318 | 2.09103 | 21 | 0.44000 | |
| | | 43.2517 | 2.09012 | 24 | 0.68000 | |
| 3 | 800 | 32.1268 | 2.78387 | 28 | 0.22800 | 35.67 |
| | | 33.4214 | 2.67894 | 100 | 0.23410 | |
| | | 35.7855 | 2.50719 | 32 | 0.22330 | |
| | | 36.6414 | 2.45057 | 23 | 0.31000 | |
| | | 46.8323 | 1.93832 | 25 | 0.21500 | |
| | | 62.9000 | | 34 | | |

Powder Diffraction Standard (JCPDS) data (cards No. 00-048-1467, 00-025-1402 and 00-043-1004), this deviation belongs due to influencing foreseen between the oxides [34,35].

**FT-IR analysis:** FTIR spectra of supported catalyst oxides ($Co_3O_4$·$Fe_3O_4$/CaO) appeared vibrations in the region 900-400 $cm^{-1}$, which can be attributed to the vibrations of M-O (where M = Co, Fe, Ca). The peak around 500 $cm^{-1}$ corresponds to a vibrational band of Ca-O bond attributed to supporter. The absorption band at 525 $cm^{-1}$ was allocated to Co-O stretching vibration mode also the corresponding peaks for Co-O bond were observed at peak locations 880 and 430 $cm^{-1}$, while the peaks at 410, 620 $cm^{-1}$ attributed to O-Fe-O bond due to resonances between centered atomic and surrounding oxygen atoms (Fig. 2). In addition, there are weak absorption bands at wave number 1630-1380 and around 3600-3400 $cm^{-1}$ matching to stretching vibration of OH groups on the surface of supported catalyst indicates the lack of presence of absorbed moisture [36-38].

**Physical properties for prepared supported catalyst:** Fig. 3 shows the physical properties of prepared catalyst at different temperature include pore volume, apparent porosity and bulk density. The best physical properties were at temperature 650 °C, which gave a high porosity and pore volume and low density and give completely convertion of hydroxides to desired spinel oxides, while at high temperature, it led to the formation of spinel $CoFe_2O_4$ /CaO because the effect of dispersion and sintering processes occurs at high calcination temperatures [39,40].

**Atomic force microscopy (AFM):** AFM images indicate to particle size for supported catalyst in three different temperatures (450, 650 and 800 ºC) found to be larger than the outcome values presence for crystallite size that measured by Debye-Scherer's equation. This means each particle consists of several crystals (polycrystals). Moreover, average of particles diameter for supported catalysts were increased with increase calcination temperatures, thus the average particle size for the catalyst at three calcination temperatures were 65.74, 75.61 and 80.00 nm), respectively (Fig. 4) [41,42].

**Energy dispersive X-ray Spectroscopy (EDS):** EDX images (Fig. 5-7) show the best temperature was 650°C which gave

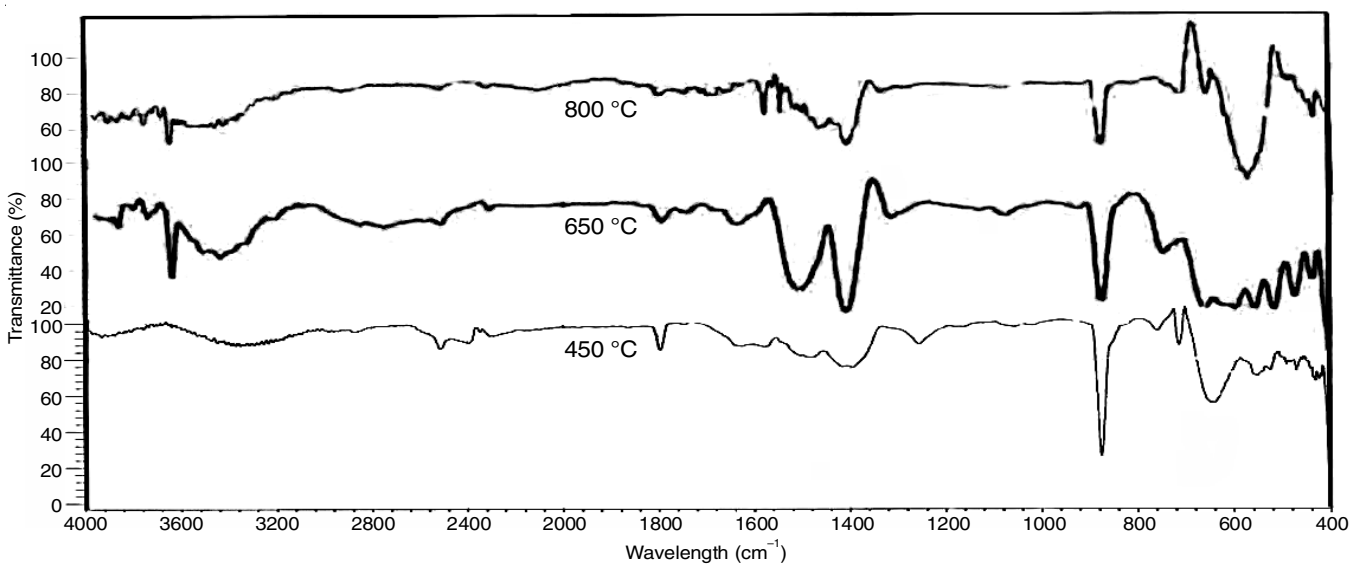


Fig. 2. FTIR spectra of the supported catalyst ($Co_3O_4$·$Fe_3O_4$/CaO)

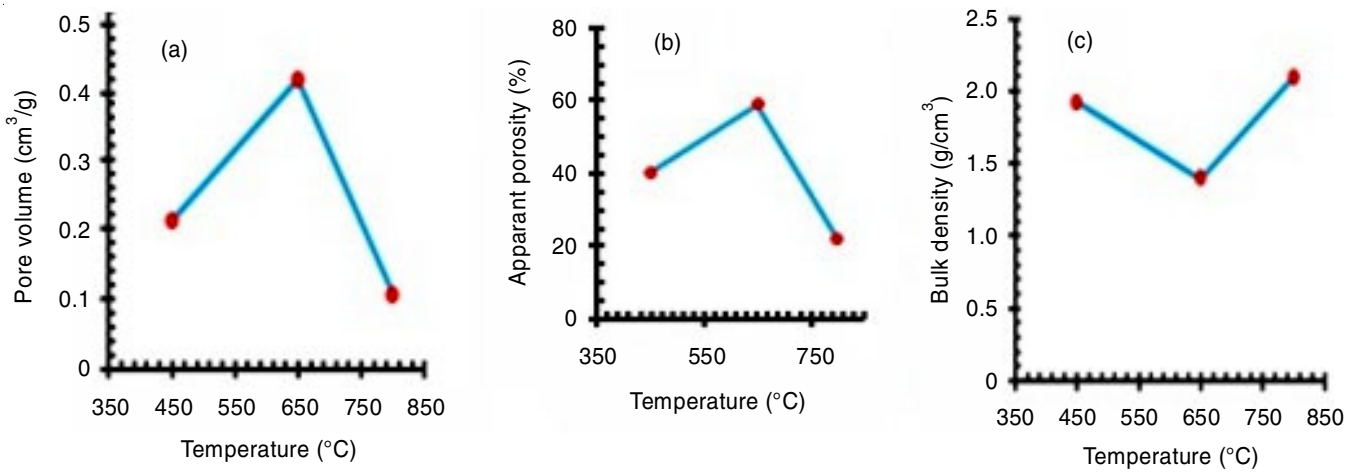


Fig. 3. Description of (a) pore volume (b) apparent porosity (c) bulk density

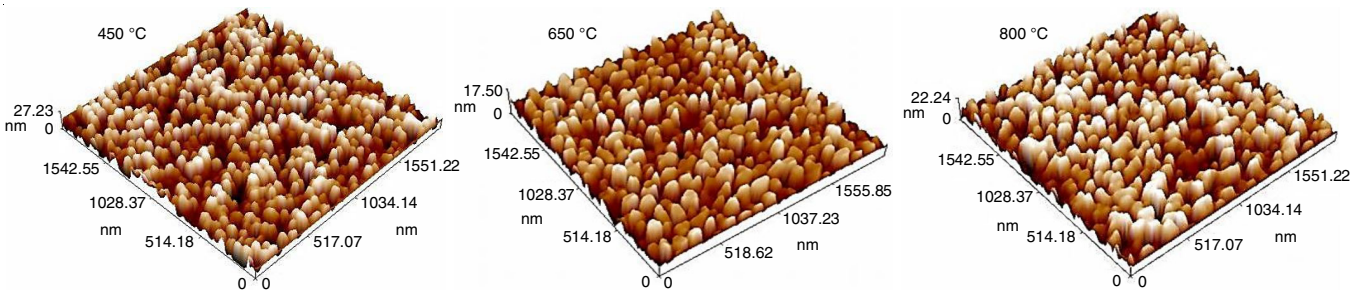


Fig. 4. AFM images of supported catalysts ($CoOFe_2O_3$·CaO) that calcination at 450, 650, 800 °C

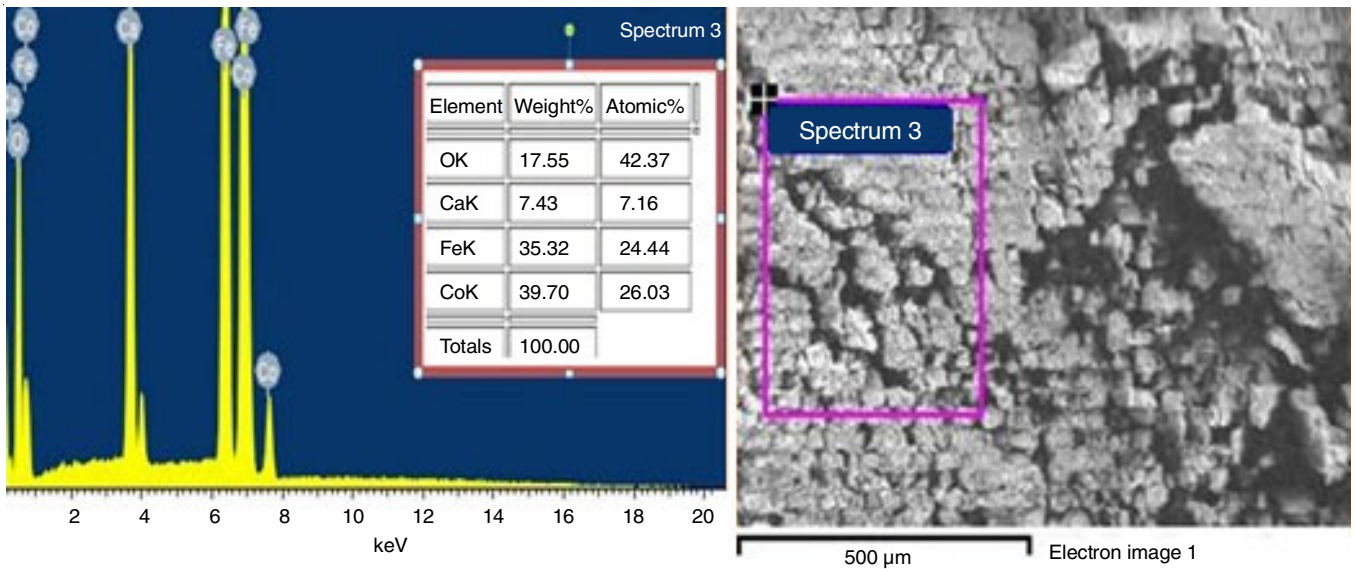


Fig. 5. EDS analyses pattern and spectrum of the supported catalyst ($Co_3O_4$·$Fe_3O_4$·CaO) at 450 °C

the best spinel phase for the prepared catalyst by matching experi-mental data with theoretical data and showed a high purity of the prepared catalyst [43].

**Atomic absorption spectrophotometry analysis:** The results of elemental analysis of cobalt, iron and calcium in the prepared catalyst prepared at different temperatures (450, 650 and 800 ºC) are shown in Table-2. Table-2 shows the excellent identical between the theoretical and experimental percentage of oxides in the prepared catalyst $Co_3O_4$·$Fe_3O_4$/CaO (25:25:50) which considered good evidence for obtained spinel type structure of the prepared catalyst.

The XRD and all spectroscopic studies results proved that the supported spinel catalyst $Co_3O_4$·$Fe_3O_4$/CaO begin to form at low temperature 450 ºC and completed at 650 ºC by using co-precipitation method and then began to convert to $CoFe_2O_4$/CaO and $FeCo_2O_4$/CaO spinel type at 800 ºC because of the increasing of dispersion of catalyst component oxides in each other with the increasing of calcination temperatures [44].

**Suggested structure of synthesized spinel type catalyst:** From the crystal field stabilization energy (CFSE) calculations for divalent and trivalent cobalt ions in spinel structure and

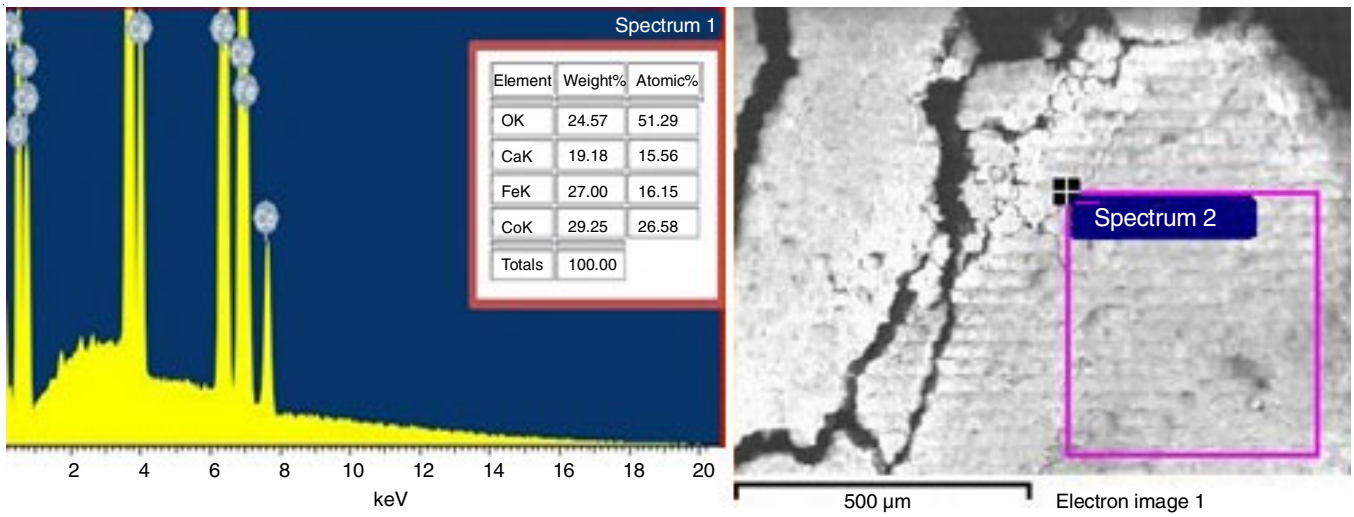


Fig. 6. EDS analyses pattern and spectrum of the supported catalyst ($Co_3O_4$·$Fe_3O_4$/CaO) at 650 °C

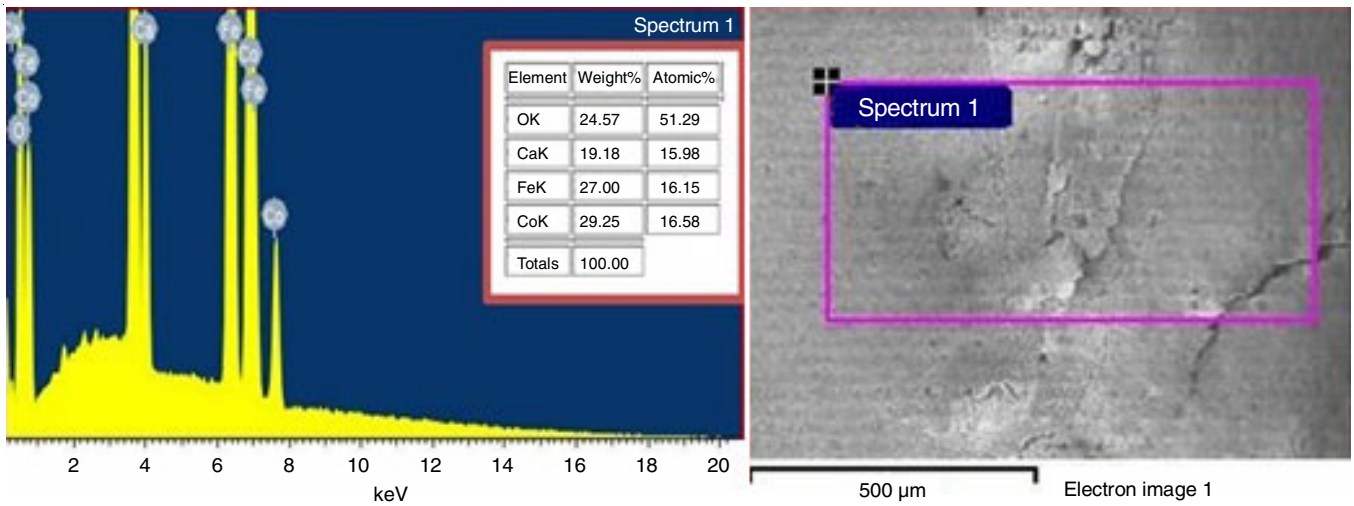


Fig. 7. EDS analyses pattern and spectrum of the supported catalyst ($Co_3O_4$·$Fe_3O_4$/CaO) at 800 °C

TABLE-2
ELEMENTAL AND OXIDES PERCENTAGE IN THE CATALYST $Co_3O_4$·$Fe_3O_4$/CaO (25:25:50)

| Oxide | Percentage of element in oxide | Percentage of oxide in the catalyst | Total practical percentage of oxide in the catalyst | Total theoretical percentage of oxide in the catalyst |
|---|---|---|---|---|
| $Co_3O_4$ | 6.0358 | 24.6600 | | |
| $Fe_3O_4$ | 6.2630 | 25.9600 | 24.66:25.96:53.6364 = 104 % | 25:25:50 = 100 % |
| CaO | 38.0333 | 53.6364 | | |

probability of existence in tetrahedral or octahedral sites in normal or inverse spinel structure locations, it is clear that a divalent cobalt ion, which is a larger than that trivalent ions and less oxidation state and has a high CFSE in tetrahedral compared to octahedral sites. Therefore it prefers a tetrahedral sites and a trivalent cobalt ions is smaller in size and has a high CFSE, when it was in octahedral sites, therefore trivalent cobalt ion located in octahedral sites in spinel structure, thus it can be concluded that normal spinel structure for $Co_3O_4[Co^{II}(Co^{III})_2O_4]$. For $Fe_3O_4$, divalent $Fe^{2+}$ has a high crystal field stabilization energy, therefore energetically prefer octahedral sites in spinel structure and half of trivalent iron ions occupy the tetrahedral sites while other occupy octahedral sites, thus the spinel structure of $Fe_3O_4$ is inverse type $Fe^{3+}$ ($Fe^{2+}$, $Fe^{3+}$)$O_4$ 45,46], also can be concluded that from the magnetic moment of all the spinel structures $[Co^{II}(Co^{III}Co^{III})_2O_4]$. $Fe^{III}(Fe^{II}Fe^{III})O_4$/CaO. The theoretical magnetic moment is in excellent agreement with the calculated magnetic moment of all spinel types in 650 ºC (Table-3).

TABLE-3
THEORETICAL AND EXPERIMENTAL MAGNETIC MOMENT FOR $Co_3O_4$·$Fe_3O_4$/CaO CATALYST AT A DIFFERENT TEMPERATURE

| Calcination temperature (°C) | $\mu_{eff}$ (B.M.) | Theoretical µ (B.M.) |
|---|---|---|
| 450 | 14.833 | 13.800 |
| 650 | 14.578 | – |
| 800 | 15.880 | – |

From the previous data, it can be concluded that the structure of spinel catalyst obtained from the interaction of normal spinel $Co_3O_4$ with inverse spinel $Fe_3O_4$ in cubic spinel structure on the surface of tetragonal CaO as shown in Fig. 8 [47,48].

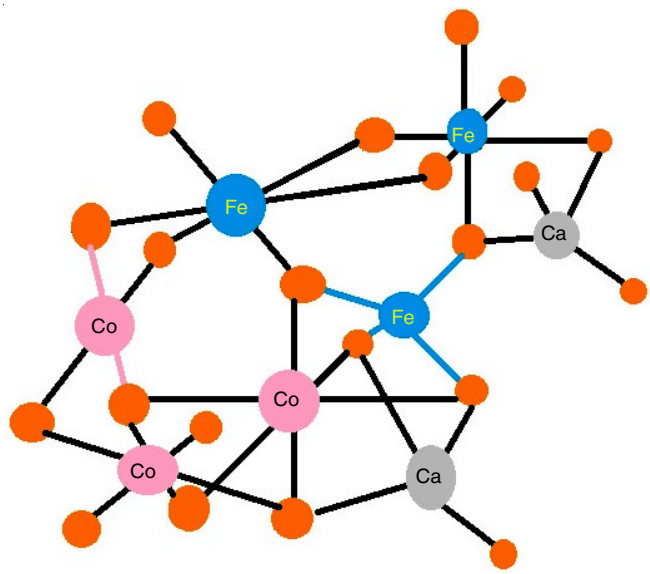


Fig. 8. Spinel structure of $Co_3O_4$·$Fe_3O_4$/CaO catalyst

**Photocatalytic activity and adsorption capacity of prepared supported $Co_3O_4$·$Fe_3O_4$/CaO catalyst:** The photocatalytic activity and adsorption capacity of the synthesized supported catalyst $Co_3O_4$·$Fe_3O_4$/CaO at three different temperature were investigated to choosing the best preparative temperature which give a high efficiency in removal of celestine blue dye (50 ppm) from the industrial textile wastewater. Fig. 9 shows that the best catalyst gives a higher activity that was prepared at 650 ºC, this may be due to the increasing of active sites and best pore size distribution in mesopores and also present the cobalt and iron in two different oxidation states which increases the efficiency of oxidation and reduction process [49].

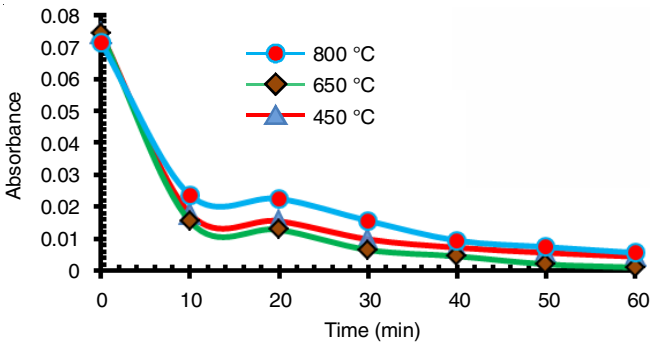


Fig. 9. Effect the better temperature of supported catalyst on the absorbance of celestine blue from aqueous solution

The effect of different weights for synthesized catalyst (0.05, 0.10, 0.15 and 0.20 g) in removal of celestine blue dye (50 ppm) was carried out by adsorption only for 10 min and then by supplying of UV light for 50 min at 25 ºC. The high removal efficiency of celestine blue dye was in 0.05 g and then decreased with the increasing weight of catalyst due to the increased solution turbidity and which resulted increase in the light scattering and thus prevented it to penetrate the inner molecules in solution, therefore the efficiency of reaction mixture decreased [50] (Fig. 10).

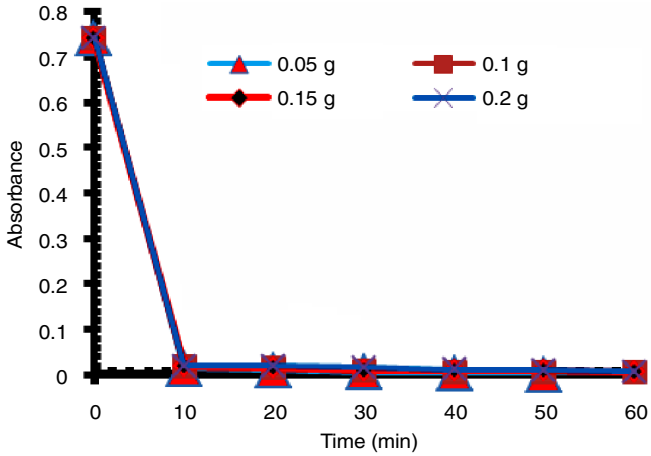


Fig. 10. Effect of the amount of supported catalyst on the absorbance of celestine blue from aqueous solution

**Reprocess of used supported catalyst:** Recycling of the supported catalyst that was previously used in the removal of celestine blue from the simulated wastewater was performed after washing several times with distilled water, then treated thermally at 250 ºC for 1 h to remove the adherent molecules of dye. The first and second usage provided the removal efficiency for dye 99.9 and 99.8 % respectively, but after third time the efficiency for removal of dye well assesses to 90 %, which can be attributed to the reduction in the active sites on the surface of the supported catalyst because of permanent adherent species of dye that may remain adsorbed on the supported catalyst [51].

## Conclusion

The obtained result proves that the supported spinel catalyst $Co_3O_4$·$Fe_3O_4$/CaO was begin to form at low temperature 450 ºC and completed at 650 ºC and then began to convert to $CoFe_2O_4$/CaO and $FeCo_2O_4$/CaO spinel type at 800 ºC. The crystalline size of the prepared catalysts were calculated by XRD (15.18, 12.17, 35.67 nm) and the average diameter particle by AFM were found to be 65.74 ,75.61 and 80.00 nm at 450, 650 and 800 ºC. respectively. The results proved that at 650 ºC, spinel phase crystalline have better activity for the removal of celestine blue dye and the best weight of catalyst was 0.05 g.

## CONFLICT OF INTEREST

The authors declare that there is no conflict of interests regarding the publication of this article.

## REFERENCES

1. R.C. Buchanan, Ceramics Materials for Electronics, Marcel Dekker: New York, edn 3 (2004).
2. F. Goga, R. Dudric, L. Bizo, A. Avram, A.H. Marincas, C. Varhely Jr. and T. Dippong, *U.B.B. Studia Chem.*, **62**, 261 (2016); https://doi.org/10.24193/subbchem.2017.1.23.
3. G. Alex, Modern Ferrite Technology, Springer, edn 2 (2006).
4. Q. Zhang, K. Singh, F. Guillou, C. Simon, Y. Breard, V. Caignaert and V. Hardy, *Phys. Rev. B*, **85**, 054405 (2012); https://doi.org/10.1103/PhysRevB.85.054405.

5. A.A. Bush, V.Ya. Shkurato, K.E. Kamentsev, A.S. Prokhorov, E.S. Zhukova, B.P. Gorshunov and V.I. Torgashev, *Phys. Rev. B*, **85**, 214112 (2012); https://doi.org/10.1103/PhysRevB.85.214112.
6. A. Maignan, C. Martin, K. Singh, C. Simon, O.I. Lebedev, *J. Solid State Chem.*, **195**, 41 (2012); https://doi.org/10.1016/j.jssc.2012.01.063.
7. A. Avnishk, S.J. Vivek, S. Kuldeep and S. Raman, *Int. J. Chem. Sci.*, **14**, 3215 (2016).
8. M.R. Kantserova, K.S. Gavrilenko, G.R. Kosmambetova, V.G. Il'in and S.N. Orlik, *Theor. Exp. Chem.*, **39**, 322 (2003); https://doi.org/10.1023/B:THEC.0000003494.21579.14.
9. A.B. Djurišic, Y.H. Leung and A.M. Ching Ng, *Mater. Horiz.*, **1**, 400 (2014); https://doi.org/10.1039/c4mh00031e.
10. E. Pelizzetti and C. Minero, *Comments Inorg. Chem.*, **15**, 297 (1994); https://doi.org/10.1080/02603599408035846.
11. T. Hisatomi, J. Kubota and K. Domen, *Chem. Soc. Rev.*, **43**, 7520 (2014); https://doi.org/10.1039/C3CS60378D.;
12. M.R. Hoffmann, S.T. Martin, W. Choi and D.W. Bahnemann, *Chem. Rev.*, **95**, 69 (1995); https://doi.org/10.1021/cr00033a004.
13. C.I. Pearce, J.R. Lloyd and J.T. Guthrie, *Dyes Pigments*, **58**, 179 (2003); https://doi.org/10.1016/S0143-7208(03)00064-0.
14. T. Robinson, G. McMullan, R. Marchant and P. Nigam, *Bioresour. Technol.*, **77**, 247 (2001); https://doi.org/10.1016/S0960-8524(00)00080-8.
15. R.S. Juang, S.H. Lin and P.Y. Hsueh, *J. Hazard. Mater.*, **182**, 820 (2010); https://doi.org/10.1016/j.jhazmat.2010.06.113.
16. U. Pagga and D. Brown, *Chemosphere*, **15**, 479 (1986); https://doi.org/10.1016/0045-6535(86)90542-4.
17. P. Borker and A.V. Salker, *Mater. Sci. Eng.*, **133**, 55 (2006); https://doi.org/10.1016/j.mseb.2006.05.007.
18. K. Golka, S. Kopps and Z.W. Myslak, *Toxicol. Lett.*, **151**, 203 (2004); https://doi.org/10.1016/j.toxlet.2003.11.016.
19. S.H. Lin and C.L. Lai, *Environ. Int.*, **25**, 497 (1999); https://doi.org/10.1016/S0160-4120(99)00015-X.
20. A. Aguedach, S. Brosillon, J. Morvan and E.K. Lhadi, *J. Hazard. Mater.*, **150**, 250 (2008); https://doi.org/10.1016/j.jhazmat.2007.04.086.
21. S. Sumathi and B.S. Manju, *Enzyme Microb. Technol.*, **27**, 347 (2000); https://doi.org/10.1016/S0141-0229(00)00234-9.
22. F. Elisangela, Z. Andrea, D.G.Fabio, R. de Menezes Cristiano, D.L. Regina and C.-P. Arturc, *Int. Biodegr. Biodegr.*, **63**, 280 (2009); https://doi.org/10.1016/j.ibiod.2008.10.003.
23. Swati, Munesh and R.C. Meena, *Arch. Appl. Sci. Res.*, **4**, 472 (2012);
24. B.H. Hameed, A.L. Ahmad and K.N. Latiff, *Dyes Pigments*, **75**, 143 (2007); https://doi.org/10.1016/j.dyepig.2006.05.039.
25. M. Meeti and T.R. Sharma, *Arch. Appl. Sci. Res.*, **3**, 849 (2012).
26. S.H.S. Chan, T.Y. Wu, J.C. Juan and C.Y. Teh, *J. Chem. Technol. Biotechnol.*, **86**, 1130 (2011); https://doi.org/10.1002/jctb.2636.
27. H.K. Salih, *Int. J. ChemTech Res.*, **9**, 754 (2016).
28. Q. Zhang, J. Yang, Y. Gao, C. Li and L. Sun, *Appl. Petrochem. Res.*, **5**, 247 (2015); https://doi.org/10.1007/s13203-015-0134-x.
29. E. Manova, D. Paneva, B. Kunev, C. Estournès, E. Rivière, K. Tenchev, A. Léaustic and I. Mitov, *J. Alloys Compd.*, **485**, 356 (2009); https://doi.org/10.1016/j.jallcom.2009.05.107.
30. Y. Devrim, E.D. Arica and A. Albostan, *Int. J. Hydrogen Energy*, **43**, 11820 (2018); https://doi.org/10.1016/j.ijhydene.2018.03.047.
31. M. Sawarkar, S.A. Pande and P.S. Agrawal, *Int. J. Eng. Technol.*, **9**, (2015).
32. A.A. Jafar and K.P. Vijaya, *J. Chem. Pharm. Res.*, **8**, 624 (2016).
33. S. Farhadi, S. Asma and J. Kosar, *J. Nanostructure*, **3**, 199 (2013); https://doi.org/10.7508/JNS.2013.02.008.
34. M.M. Sahasrabudhe and G.R. Pathade, *Arch. Appl. Sci. Res.*, **3**, 403 (2011).
35. N. Chiwaye, L.L. Jewell, D.G. Billing, D. Naidoo, M. Ncube and N.J. Coville, *Mater. Res. Bull.*, **56**, 98 (2014); https://doi.org/10.1016/j.materresbull.2014.04.065.
36. N.D. Kandpal, N. Sah, R. Loshali, R. Joshi and J. Prasad, *J. Sci. Ind. Res. (India)*, **73**, 87 (2014).
37. R. Manigandan, K. Giribabu, R. Suresh, L. Vijayaakshmi, A. Stephen and V. Naraayanan, *Chem. Sci. Trans.*, **2S1**, S47 (2013); https://doi.org/10.7598/cst2013.10.
38. A. Azam, A.S. Ahmed, M. Oves, M.S. Khan, S.S. Habib and A. Memic, *Int. J. Nanomed.*, **7**, 6003 (2012); https://doi.org/10.2147/IJN.S35347.
39. C.N. Satterfield and N. Cahrles, Heterogeneous Catalysis in Practice, McGraw-Hill Inc.: New York, p. 106 (1980).
40. C.L. Thomas, Catalytic Process and Proven Catalyst, Academic Press: New York, p. 68 (1970).
41. M.A. Luma, I. Irina, H.H. Falah and W.B. Detlef, *Int. J. Photoenergy*, **Article ID 503516** (2014); https://doi.org/10.1155/2014/503516.
42. M.K. Sanjay, H.V. Jadhav, S.V. Bangale, P.N. Jagdale and R.B. Sambhaji, *Adv. Appl. Sci. Res.*, **2**, 252 (2011).
43. Z.Z. Lazarevic, C. Jovalekic, D. Sekulic, M. Slankamenac, M. Romcevic, A. Milutinovic and N.Z. Romcevic, *Sci. Sinter.*, **44**, 331 (2012); https://doi.org/10.2298/SOS1203331L.
44. G. Godillot, L. Guerlou-Demourgues, L. Croguennec, K.M. Shaju and C. Delmas, *J. Phys. Chem.*, **117**, 9065 (2013); https://doi.org/10.1021/jp3100359.
45. F.J. Manjon, I. Tiuinyanu and V. Ursaki, Pressure-Induced Phase Transitions in AB2X4 Chalcogenide Compounds, Springer Series in Materials Science, vol. 189 (2014).
46. M.Y. Arsent'ev, N.Y. Koval'ko, A.V. Shmigel', P.A. Tikhonov and M.V. Kalinina, *Glass Phys. Chem.*, **43**, 376 (2017); https://doi.org/10.1134/S1087659617040022.
47. G. Blasse, *Philip Tech. Rev.*, **28**, 23 (1967).
48. S.H. Kadhim, *Asian J. Chem.*, **30**, 1650 (2018); https://doi.org/10.14233/ajchem.2018.21425.
49. N.R. Jana, Y.F. Chen and X.G. Peng, *Chem. Mater.*, **16**, 3931 (2004); https://doi.org/10.1021/cm049221k.
50. R.M. Mohamed, I.A. Mkhalid and E.S. Baeissa, *J. Nanotechnol.*, **Article ID 329082** (2012); https://doi.org/10.1155/2012/329082.
51. M. Argyle and C. Bartholomew, *Catalyst*, **5**, 145 (2015); https://doi.org/10.3390/catal5010145.